Interfacial engineering and coupling of electric and magnetic properties in $Pb(Zr_{0.53}Ti_{0.47})O_3/CoFe_2O_4$ multiferroic epitaxial multilayers

J. X. Zhang, J. Y. Dai,[a] and H. L. W. Chan
Department of Applied Physics, The Hong Kong Polytechnic University, Hung Hom, Kowloon, Hong Kong, People's Republic of China

(Received 10 December 2009; accepted 13 March 2010; published online 20 May 2010)

Epitaxial magnetoelectric (ME) $Pb(Zr_{0.53}Ti_{0.47})O_3$(PZT)/$CoFe_2O_4$(CFO) multilayer nanocomposite thin films with up to 11 alternative layers are grown on Nb doped $SrTiO_3$ (STO) substrates by pulsed-laser deposition. X-ray diffraction and high resolution transmission electron microscopy studies reveal a good epitaxial relationship between the PZT and CFO layers without interfacial reaction at their interfaces. These epitaxial composite films exhibit strong ferroelectric and magnetic responses simultaneously at room temperature, and the interfacial-coupling-modulated dielectric behavior, polarization, and magnetic properties are observed and analyzed systematically. These results suggest that the magnetic, electric, and ME coupling effect may be tuned by the "strain engineering" in ferroelectric/magnetic or other multiferroic superlattice. © *2010 American Institute of Physics*. [doi:10.1063/1.3386510]

I. INTRODUCTION

Magnetoelectric (ME) nanocomposite materials have attracted a great deal of attention due to their potential applications in many multifunctional devices such as nonvolatile memory,[1,2] which may not be realized in their bulk counterparts. The observation of ME coupling in the self-assembled multiferroic $BaTiO_3$(BTO)/$CoFe_2O_4$(CFO) nanostructures[3] motivated a broad range of research in multiferroic nanocomposites from the aspect of experimental characterization[4,5] and theoretical calculation.[6] Enhanced polarization observed in ferroelectric superlattice[7] may provide a new route to multiferroic superlattice structure.[8] Therefore, the interfacial effects may play a critical role in deciding the intrinsic ferroelectric, magnetic, and even the ME coupling in the interface of ferroelectric/magnetic heterostructure. The observation of large magnetic-field-influenced polarization in $La_{0.6}Sr_{0.4}MnO_3/0.7Pb(Mg_{1/3}Nb_{2/3})O_3-0.3(PbTiO_3)$ superlattice may give the evidence of strong coupling in the interface between ferroelectric and magnetic constituents.[9]

Furthermore, the strong influence of lattice strain on the magnetic properties of BTO/CFO nanostructure[10] and the sequence-dependent ferroelectric properties in sol-gel derived polycrystalline $Pb(Zr_{0.53}Ti_{0.47})O_3$ (PZT)/CFO multilayers[11] may predict that the ME property significantly depend on the interfacial coupling between piezoelectric and magnetic phases, especially when the dimension of materials is reduced to nanoscale or atomic scale.[12] Ortega *et al.*[13] reported the Maxwell–Wagner space charge effects on PZT/CFO polycrystalline multilayers and the corresponding ME effect.[14] But the discussion of the influence of interfacial coupling strain on the electric and magnetic properties in epitaxial PZT/CFO multilayer nanocomposite is rare, unlike the deeply studied ferroelectric/ferroelectric and ferroelectric/dielectric superlattice.[7,15] In this article, the epitaxial PZT, CFO pure film, and PZT/CFO multilayers were deposited in order to give the insight into the influence of perovskite/spinel interface and residual strain on the electric and magnetic properties. The comparison of electric and magnetic between single phase and multilayers with the same volume fraction was carried out and analyzed. This interfacial engineering in perovskite/spinel heterostructure will provide an understanding and an additional degree of freedom to control the ferroelectric, magnetic, and ME interfacial coupling in epitaxial multilayer and superlattice multiferroics.

II. EXPERIMENTAL DETAILS

PZT, CFO single-phase, and PZT/CFO epitaxial multilayer nanocomposite thin films with 3, 5, and 11 layers, respectively, were deposited on 0.5-mm-thick (001)-oriented Nb:STO single crystal substrate by pulsed-laser deposition (PLD) using a KrF exciter laser of 248 nm in wavelength, 5 Hz in repetition rate, and 2.50 J/cm^2 in laser energy density. The oxygen pressures used for depositing the alternate PZT and CFO layer was 13 Pa and substrate temperature was 600 °C, respectively. The stoichiometric targets of CFO and PZT were prepared through a standard solid reaction sintering processing. In the PZT target, over 10% of Pb was added to avoid Pb deficiency due to its volatilization during sintering and depositing. In the multilayer structure, the first and the final layers are kept as PZT. We carefully control the total thickness (360 nm) and the volume fraction (2/3 for PZT) in all samples as the constant in order to diminish other influences on the intrinsic electric and magnetic properties other than the interface effect.

III. RESULTS AND DISCUSSION

A. Structure and morphology

The structural characterization of the composite thin films was carried out by x-ray diffraction (XRD) pattern us-

[a]Author to whom correspondence should be addressed. Electronic mail: apdaijy@inet.polyu.edu.hk.

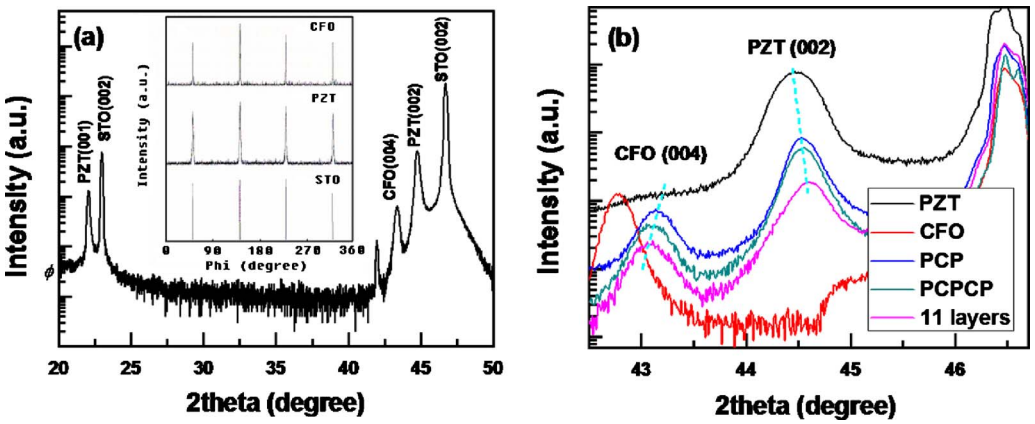

FIG. 1. (Color online) (a) The XRD patterns of 11-layer PZT/CFO epitaxial multilayers, the inset gives the scan results and (b) the XRD θ-2θ scan of PZT, CFO, and PZT/CFO composite films with different number of layer.

ing a Bruker D8 discover XRD system equipped with copper radiation. The in-plane lattice parameters were evaluated by d-spacing of (001) and (011) plane. As shown in Fig. 1(a), only (00*l*) diffraction peaks for CFO and PZT were observed in the diffraction pattern of θ-2θ scan of 3, 5, and 11 layers thin films, following those of the single crystal STO substrate, which confirms the c-axis orientation of the PZT/CFO multilayered films without any contribution from a-axis oriented domains and impurity phases. The cubic-on-cubic epitaxial relationship between PZT, CFO, and STO substrate with fourfold symmetry has been confirmed by XRD ϕ scan in the inset of Fig. 1(a). The scan data were recorded around the CFO (044), PZT (022), and STO (022) reflections, which show a set of four distinct peaks with 90° of separation. From the XRD patterns of θ-2θ scan around 42° to 47°, Fig. 1(b), the CFO and PZT peaks in multilayer structure shift to the large angle region from their respective single phase films, which indicates the release of in-plane compressive strain in multilayers. Due to the mismatch of in-plane lattice constant of PZT (a=0.405 nm), CFO (a=0.839 nm), and STO (a=0.391 nm) for respective bulk materials, the epitaxial single-phase PZT and CFO films grown on STO substrate will suffer the in-plane compressive strain. However, with the alternative growth of PZT and CFO, the inserted PZT or CFO can serve as the buffer materials for their following layer each other, which benefits the release of in-plane compressive strain in both PZT and CFO. Therefore, the peak in multilayer shifts right compared to that of single phase films. When the thickness of each layer is reduced (up to 30 nm for each layer in 11 layer film), the strain due to the lattice mismatch cannot be completely released in PZT, which helps restore the in-plane compressive strain in the CFO layer. Because the unreleased strain can reduce the difference of the a-axis lattice constant of PZT and CFO layer, the difference of c-axis lattice constant of PZT and CFO will increase. Consequently, the fact that peaks of CFO and PZT shift to the opposite directions with the increased number of layer indicates that the residual strain is strongly influenced by themselves in multilayers but not the STO substrate. The interfacial coupling effect and lattice strain is modulated by the strain engineering in each phase. The measured lattice constant of PZT and PZT/CFO multilayers are included in Table I.

The morphology and the interfacial structure of the multilayered epitaxial films were studied by high resolution transmission electron microscopy (HRTEM, using a JEOL 2010 electron microscope operated at 200 kV). Figures 2(a) and 2(b) are low-magnetization cross-sectional bright-field images of the PZT/CFO films with 3 and 11-layers on STO single crystal substrates, where the thickness of the films is of 360 nm in all samples. The relatively dark area corresponds to the PZT phase due to the relatively heavy elements. The clear interfacial structure revealed by high resolution electron microscope and the selected area electron diffraction pattern (SAED), shown in Figs. 2(c) and 2(d), further confirm the heteroepitaxial growth of PZT/CFO multilayer on (001) STO substrate even after the growth of 11 alternative layers.

B. Strain-dependent dielectric and ferroelectric properties

In order to carry out the electrical property measurements, Pt dot electrode with a diameter of 0.2 mm was deposited on the top surface of the thin films by PLD. Current density-voltage (J-V) characteristic curve was measured by Keithley (2410 sourcemeter). Spectroscopic dielectric behaviors of the nanocomposite films were measured by an imped-

TABLE I. The in-plane and out-of-plane lattice constant of PZT and the PZT/CFO multilayers.

	PZT	3-layer	5-layer	11-layer	Cubic PZT
a (Å)	4.027	4.032	4.035	4.041	4.050
c (Å)	4.071	4.066	4.064	4.059	4.050
$d_{(011)}$ (Å)	2.863	2.862	2.864	2.864	2.864

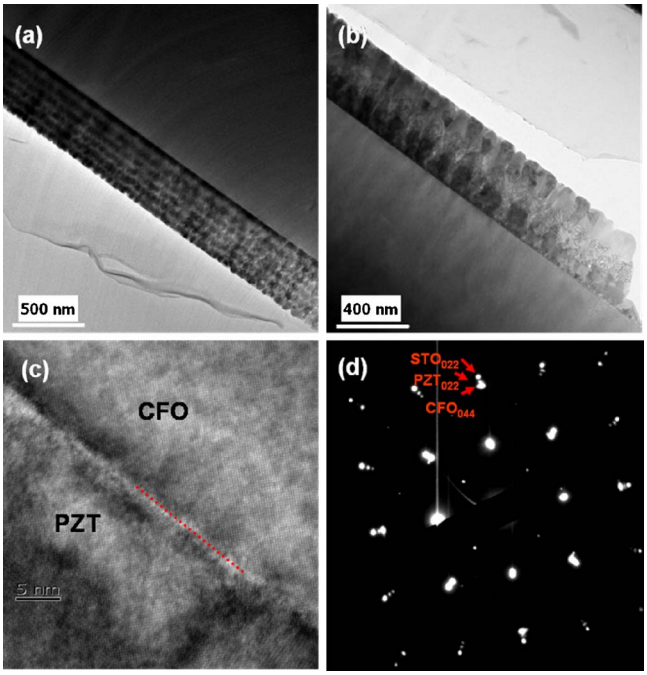

FIG. 2. (Color online) [(a) and (b)] The low-magnification TEM images of 11-layer and 3-layer PZT/CFO nanocomposite films, (c) the HRTEM image of interfacial structure of PZT/CFO, and (d) the SAED pattern including PZT, CFO, and STO substrate.

ance analyzer (Agilent 4294A). The ferroelectric hysteresis loops of the PZT/CFO multilayered thin films were measured using a ferroelectric tester (TF Analyzer 2000, aixACCT) at 1 kHz. We measure the dielectric and ferroelectric properties along the thickness direction (ε_{33}) and (P_3) with the conductive Nb:STO bottom electrode substrates. In our experiments, the electrode/PZT interface is kept unchanged so that the changes in the dielectric behavior, ferroelectric properties, and leakage current originate from the intrinsic nature of the multilayer but not due to any phenomena occurred at the electrode/film interface.

Since there are space charges exist in the PZT/CFO polycrystalline multilayer films,[13] we first measure dielectric constant of PZT and CFO single phase films in order to compare and evaluate theoretically the dielectric behaviors in the epitaxial multilayer. Therefore, we obtain the theoretical dielectric constant (ε_{33}) and ac conductance (σ) of PZT/CFO multilayer capacitors from Maxwell–Wagner space charge model, as follows:

$$\varepsilon = \frac{\varepsilon_C \omega E_0 - \phi_P \sigma_C B - \phi_P \varepsilon_C A \omega}{\phi_C \omega E_0} = \frac{B\sigma_P + A\varepsilon_P \omega}{\omega E_0}, \tag{1}$$

$$\sigma = \frac{\sigma_C E_0 - \phi_P \sigma_C A + \phi_P \varepsilon_C B \omega}{\phi_C E_0} = \frac{A\sigma_P - B\omega E_P}{E_0}, \tag{2}$$

where

$$A = \frac{\sigma_C \tau + \varepsilon_C \omega^2 \tau^2}{(\phi_P \varepsilon_C + \phi_C \varepsilon_P)(1+\omega^2\tau^2)} E_0, \tag{3}$$

and

$$B = \frac{(\varepsilon_C - \sigma_C \tau)\omega\tau}{(\phi_P \varepsilon_C + \phi_C \varepsilon_P)(1+\omega^2\tau^2)} E_0, \tag{4}$$

and

$$\tau = \frac{\phi_P \varepsilon_C + \phi_C \varepsilon_P}{\phi_P \sigma_C + \phi_C \sigma_P}, \tag{5}$$

where the E_0 (500 mV) is the external electric field we applied during dielectric constant measurement. We neglect the influence of this small external electric field on the remnant polarization of multilayers. $\phi_P = 2/3$ and $\phi_P = 1/3$ (symbol P and C indicate PZT and CFO). The σ in each material is derived by the dielectric loss $\sigma = \varepsilon_0 \varepsilon' \omega \tan \delta$.

Figure 3 shows the theoretical calculation and experimental observation of dielectric constant and dielectric loss in single PZT, CFO films, and multilayer capacitors. The calculated results are in agreement with our experimental observation of 3-layer, 5-layer, and 11-layer PZT/CFO nanocomposites. Therefore, we conclude that the peak of dielectric loss at a relatively low frequency should be originated from the space charge effect in the multilayered films, while the dielectric loss peak in pure CFO film should originate from the electrode/CFO interface and CFO itself, which is the same with other report in the polycrystalline systems.[16] In addition, the dielectric loss peak is not shown in pure PZT film which has the same contact of sample and electrode with the mutilayer structure. We can further rule out the possibility that the space charge is dominated in the interface of

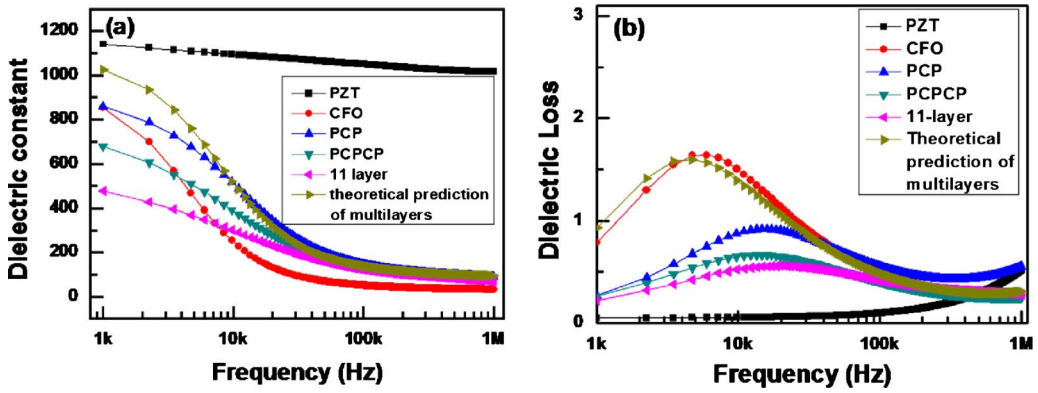

FIG. 3. (Color online) Experimental observation and theoretical prediction of spectroscopic dielectric constant (a) and dielectric loss (b) of PZT, CFO, and PZT/CFO multilayer thin films.

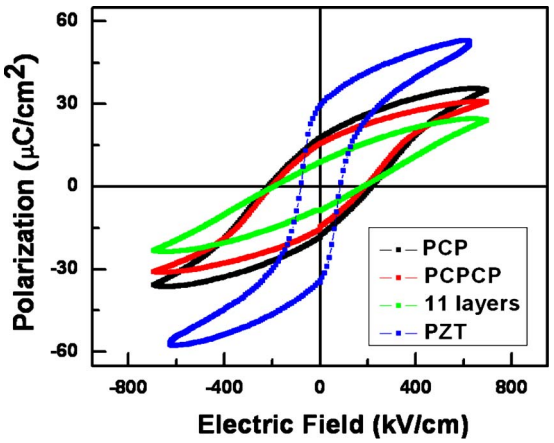

FIG. 4. (Color online) Ferroelectric hysteresis loops of the PZT film and the PZT/CFO multilayered composite films.

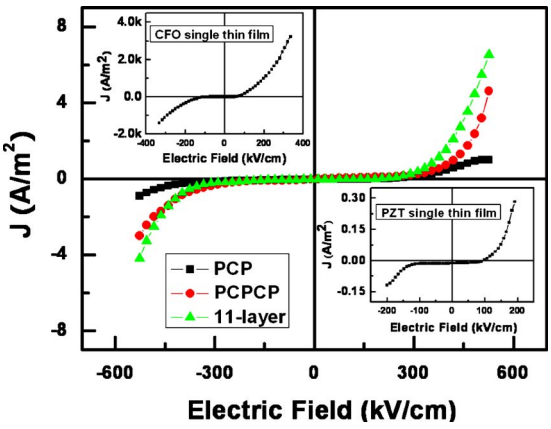

FIG. 5. (Color online) Electric field dependent-leakage current density curves of the PZT/CFO multilayered composite films, where the inset denote the leakage current density curves of the single layer PZT and CFO films.

electrode and films. However, from the Eqs. (1) and (2), ε_{33} and σ can only be viewed as a function of volume fraction, dielectric constant, and ac conductivity in each phase. Since we make the volume fraction constant in the multilayered structure, the space charge and dielectric behavior should be independent on the number of interface of PZT/CFO epitaxial multilayer. But phenomenally, from the dielectric loss peaks, especially in a relatively low frequency, we observe that the space charge effect is reduced with the increase in the number of layers, which is different from the discussion of PZT/CFO polycrystalline multilayer.[13] Zubko *et al.*[17] and Pertsev *et al.*[16] mentioned that the effect of strain will be to rescale the local Landau coefficients α and β. The effective coefficients describing the dielectric susceptibility and polarization will also be rescaled. Therefore, the in-plane compressive stress in the epitaxial structure may influence the polarization behavior near the interfacial region, which will in turn, influence the distribution of space charge[18] and be responsible for the observed dielectric nature of PZT/CFO multilayer nanocomposite films.

To further study the number of layer-dependent polarization in epitaxial PZT/CFO multilayer, the ferroelectric hysteresis (P-E) loops of the PZT/CFO multilayered thin films were measured. Figure 4 gives the P-E loops of PZT single phase, 3-layer, 5-layer, and 11-layer composite thin films, and the corresponding remnant polarizations are 31.8 $\mu C/cm^2$, 17.9 $\mu C/cm^2$, 15.3 $\mu C/cm^2$, and 8.5 $\mu C/cm^2$, respectively. The coercive field increases from 80 kV/cm for the PZT film to 200 kV/cm for the multilayered film. Since the coercive field of each PZT layer in the composite film should be a function of external electric field, volume fraction, and dielectric constant of PZT and CFO, if we neglect the conductivity of the multilayer, the actual electric field applied on each PZT layer can be described by

$$E_P = \frac{E_m}{\phi_p + \phi_c \frac{\varepsilon_p}{\varepsilon_c}}, \tag{6}$$

where E_m and E_p are the electric field applied on the multilayers and the field applied on each PZT layer, respectively, ϕ_p, ϕ_c, ε_p, and ε_c are the volume fractions and dielectric constants of the PZT and CFO layers in the film. Therefore, we have to increase the external field in the multilayers in order to maintain the switching electric field in each PZT layer. It is easy to understand the significant enhancement of the coercive field in the film compared to those in the single phase PZT film. This behavior is consistent with the typical leakage current densities as a function of voltage (J-V), as shown in Fig. 5. The breakdown voltage of multilayer is much higher than the one of single layer PZT film (inset in Fig. 5). The leakage current density of PZT, CFO, and the multilayers under an electric field of around 200 kV/cm are 0.2 A/m^2, 1000 A/m^2, and 0.3 A/m^2, respectively. We can also observe that the leakage current density in the multilayers is comparable to the one of PZT film around the same electric field in spite of the insert of relatively low resistive CFO. The robust insulating behavior is required to sustain a ferroelectric polarization and predict a tolerable poling process for the further ME coupling output.

To give a theoretical evaluation of the number-of-layer-dependent polarization in the multilayered thin films and compare with our experimental observation, we estimate the average residual stress suffered by the PZT phase in the epitaxial multilayers from the XRD result. The in-plane a-axis lattice parameters in PZT layer increase from 4.027 to 4.032, 4.035, and 4.041 Å, which corresponding to single PZT, 3-layer, 5-layer, and 11-layer films, shown in Table I. The Young's modulus of the epitaxial $Pb(Zr_{0.52}Ti_{0.48})O_3$ film was 92.6 GPa which was reported elsewhere.[19] Therefore, the residual in-plane compressive stress suffered by the corresponding epitaxial PZT films should be −520, −410, −330, and −204 MPa, while for the cubic PZT bulk materials without residual stress, the lattice constant a=4.05 Å.[20] We adopt Landau–Devonshire's phenomenological thermodynamic formalism method to calculate the spontaneous polarization,[21] therefore we have expression

$$P_3^2 = \frac{-\alpha_{11} + \sqrt{\alpha_{11}^2 - 3\alpha_{111}(\alpha_1 - 2Q_{12}\sigma)}}{3\alpha_{111}}, \tag{7}$$

where P_i is the magnitude of the polarization vector along the direction i, α_i is the dielectric stiffness, α_{ij}, α_{ijk} are the

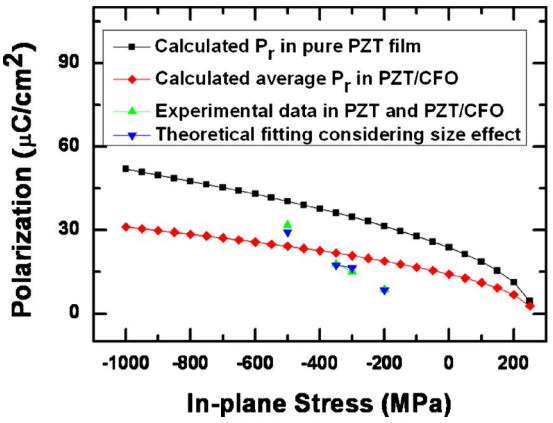

FIG. 6. (Color online) Theoretical calculation of in-plane stress-dependent polarization in pure PZT film, PZT/CFO multilayers, simulated results of polarization considering size effect in each PZT layer, and our experimental fitting in PZT single-phase film and 3-layer, 5-layer, and 11-layer PZT/CFO nanocomposite thin films.

high-order stiffness coefficients at constant stress, and Q_{11}, Q_{12}, and Q_{44} are the electrostrictive coefficients written in polarization notation. The dielectric stiffness and electrostrictive coefficients of PZT films are given in a series of papers.[22]

In addition, according to the discussion of the "dilution" of the effect of ferroelectric materials in a dielectric matrix in the BTO–STO–CTO superlattice,[7] when we consider the influence of the nonferroelectric layer, the electric displacement should be expressed by

$$D = \frac{\varepsilon_P \varepsilon_C}{\phi_C \varepsilon_P + \phi_P \varepsilon_C} E + \left(1 - \frac{\phi_C \varepsilon_P}{\phi_C \varepsilon_P + \phi_P \varepsilon_C}\right) P_P, \tag{8}$$

where D and P are the electric displacement and polarization of the multilayers, respectively. Then the average polarization in the electrostatic model can be derived

$$P_m = \frac{P_p}{1 + \frac{\phi_c}{\phi_p} \times \frac{\varepsilon_p}{\varepsilon_c}}. \tag{9}$$

Therefore, we obtain the polarization of the multilayers

$$P_m = \frac{\sqrt{\frac{-\alpha_{11} + \sqrt{\alpha_{11}^2 - 3\alpha_{111}(\alpha_1 - 2Q_{12}\sigma)}}{3\alpha_{111}}}}{1 + \frac{\phi_c}{\phi_p} \times \frac{\varepsilon_p}{\varepsilon_c}}, \tag{10}$$

where P_m is the average polarization of the PZT/CFO multilayered films, P_P indicates the polarization in each PZT layer.

Figure 6 shows the theoretical calculation and experimental observation of the spontaneous polarization for the thin films with different in-plane compressive stresses. Our theoretical prediction describes the remnant polarization decrease with the release of in-plane compressive stress, qualitatively interpreted our experimental data. We consider the influence of the dielectric matrix in the PZT/CFO multilayers according to Eq. (10). The addition of nonferroelectric phase reduces the average polarization, compared to the pure PZT films suffered from different in-plane stresses. It is easy to understand the dramatic decrease in the polarization from single layer PZT film to the multilayered films as what we observed. In addition, the size effect discussed extensively by other reports in ferroelectric layer may be another factor to induce the decreased polarization in multilayers.[23] The remnant polarization when we consider the size effect in each PZT layer will be expressed by

$$P_r = \frac{1}{R}\sqrt{\frac{\alpha_0(T_c - T)}{\beta}}, \tag{11}$$

where α_0 and β are the modified and original Landau parameters, respectively.

$$R = \frac{3(L + 4\delta)}{2(L + 6\delta)}, \tag{12}$$

$$T_c = T_0 - \frac{32\kappa(L + 3\delta)}{3\alpha_0 L(L + 4\delta)^2}, \tag{13}$$

where L denotes the thickness of PZT layer and δ is the so-called extrapolation length of the PZT/CFO interface, T_0 is the Curie temperature of bulk PZT, and κ is the positive constant and represents the contribution from the spatial variation in polarization. When we take all of the above parameters,[23–26] shown in Table II, the theoretical fitting considering the size effect is in agreement with our experimental observation. Therefore, we may conclude that (1) the Maxwell–Wagner space charge effect exists in the epitaxial interface of the PZT and CFO layers. (2) The decreased dielectric constant and the remnant polarization with the increased number of interfaces most possibly originate from the release of residual stress in the multilayered films. (3) Size effect also exists in our experimental observation and theoretical calculations.

C. Strain-dependent magnetic properties

The magnetic properties of the PZT/CFO multilayer films were characterized by a vibrating sample magnetometer (Lakeshore, Model 7300 series). The accurate volumes of the thin films are required to calculate magnetization, which is equal to the area of the substrate times the thickness of the films. Field-dependent magnetization at room temperature was measured by applying the magnetic field parallel to the plane of the films with the measurement up to a field of 796 kA/m. The saturated magnetizations are 0.082, 0.099, and 0.116 T for 3-layer, 5-layer, and 11-layer PZT/CFO epitaxial

TABLE II. The values of parameters used in calculating the polarization of PZT and PZT/CFO multilayers.

α_1(m F^{-1})	α11(m^5 C^{-2} F^{-1})	α_{111}(m^9 C^{-4} F^{-1})	Q_{12}(m^4 C^{-2})	L	δ	α_0	β	T_0	κ
-8×10^6	7.12×10^7	2.35×10^6	-1.54×10^{-02}	1	4	1	1	1	1

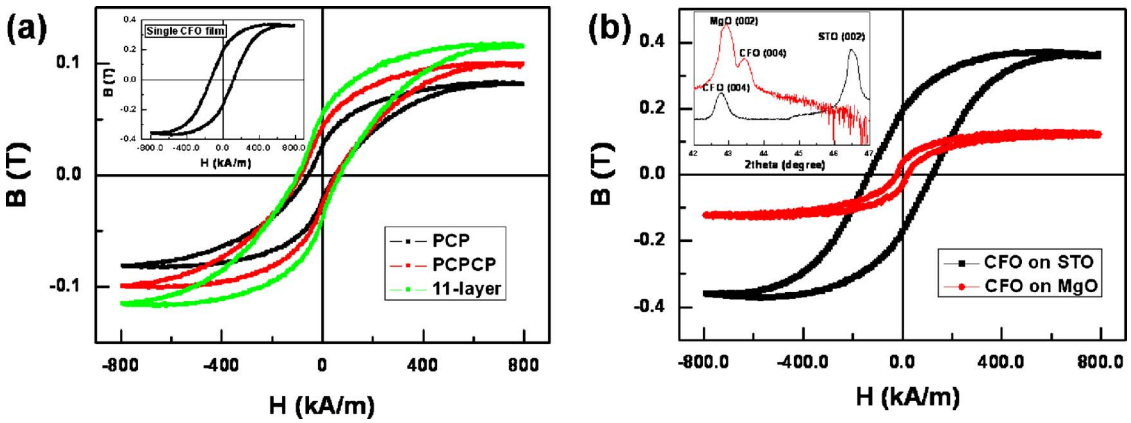

FIG. 7. (Color online) (a) Magnetization hysteresis loops of single-phase CFO (the inset) and PZT/CFO multilayered thin films grown on STO substrates and (b) magnetization hysteresis loops of expitaxial CFO thin films grown on STO and MgO substrates (the inset shows the corresponding θ-2θ XRD patterns where the lattice constant in each sample can be derived).

films, respectively, which are comparable to the value of the single layer $CoFe_2O_4$ epitaxial film [the inset of Fig. 7(a)] if we consider the volume fraction (1/3 for CFO) in the multilayers. The in-plane coercive fields for single layer CFO film, 11-layer, 5-layer, and 3-layer films were 129.0, 84,8, 67.7, and 54.1 kA/m, respectively.

Similar to the evaluation of lattice constant in the PZT layers, the CFO layers suffer from the strong in-plane compressive strain due to the 7.4% lattice mismatch with the bare (001) STO substrate. In the PZT/CFO multilayers, the PZT layer can serve as a buffer layer (bulk lattice constant a =4.036 Å) to release the lattice mismatch between the CFO layers (bulk lattice constant a=8.396 Å) and the STO (bulk lattice constant a=3.90 Å) substrate. However, with the increase in number of layers, i.e., the reduction in the thickness in each layer, the in-plane compressive strain from the PZT layer in the 11-layer film cannot be released as much as the one in the 3-layer film, helping restore the in-plane strain during the growth of the following layers. Consequently, the in-plane compressive strain will be retained with the increased number of layers. This is consistent with our XRD and transmission electron microscopy (TEM) analysis, the a-axis lattice constant of the CFO layers decreases from 8.371 Å to 8.363 Å and 8.352 Å when the number of layers increases from 3 to 5 and 11, indicating the increase of in-plane compressive strain in the CFO layers when the number of layers increases. The lattice constant and corresponding magnetic parameters are shown in Table III.

The above residual strain and structure dependent magnetization was also observed in other epitaxial ferrite thin films.[27,28] The enhanced magnetic anisotropy in BTO–CFO nanostrucuture[10] originated from the out-of-plane compressive strain suffered by CFO phase. Hu *et al.*[29] have found that both external stress and cation distribution can be responsible for the anomalous magnetic behavior in CFO epitaxial films. Since we control the volume fraction and other conditions as constant during the thin film growth except the number of layers and the thickness in each phase, cation distribution should be the same in each layer. Therefore, we conclude that the number of layers-dependent coercive field and magnetization should be attributed to the in-plane compressive stress in CFO phase induced by the neighboring PZT layers. This stress-induced magnetic property in the present CFO epitaxial films is consistent with the report by Wakiya.[28]

To further prove the strain-induced magnetization in CFO films, we fabricated and characterized the epitaxial CFO thin film on MgO (a-axis lattice constant=8.396 Å) substrate under the same condition as on STO substrate. Figure 7(b) shows the in-plane magnetic hysterisis loops of CFO grown on STO and MgO substrates. From the XRD data [the inset of Fig. 7(b)], we can obtain that the a-axis lattice constant of CFO is 8.343 Å grown on STO which suffering an in-plane compressive stress, while it is 8.413 Å grown on MgO substrate, with a tensile stress. The saturated magnetization and coercive field of CFO on MgO are 0.121 T and 21.9 kA/m. The coercive field is dramatically lower than the values of CFO on STO. The coercive field and magnetization of CFO on MgO are also lower than the value of 3-layer structure if we consider the volume fraction of CFO in nano-

TABLE III. In-plane and out-of-plane lattice constants, saturated magnetization, and coercive field of the CFO films and multilayers.

Sample	d_{001} (Å)	d_{011} (Å)	d_{010} (Å)	in-plane strain (%)	B (T)	H_c (kA/m)
CFO on STO	8.449	5.937	8.343	−0.631	0.364	129.0
11-layer	8.418	5.929	8.352	−0.524	0.347	84.8
5-layer	8.412	5.931	8.363	−0.393	0.298	67.7
3-layer	8.403	5.930	8.371	−0.297	0.245	54.1
CFO on MgO	8.326	5.918	8.413	0.202	0.121	21.9

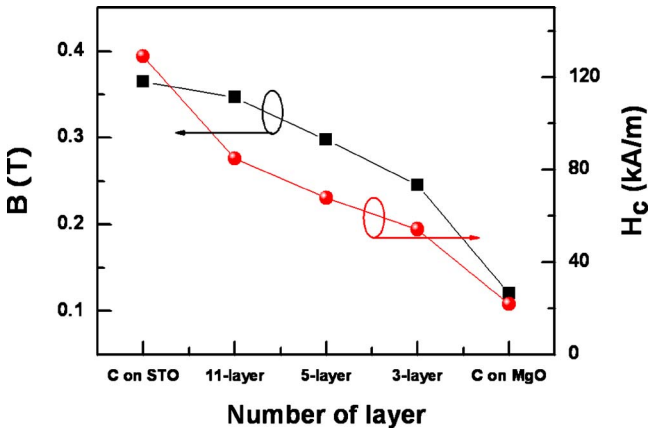

FIG. 8. (Color online) In-plane strain dependent magnetic behaviors in CFO and CFO/PZT multilayers grown on STO substrate and CFO grown on MgO substrate.

composite. This is in good agreement with our previous observation: the decrease of in-plane compressive stress or the increase of in-plane tensile strain will reduce the magnetization and coercive field of CFO films. Since we compare the in-plane directions, the demagnetization energy factor does not play a critical role in all of the cases here.[29] A plot of the saturated magnetization and coercive field against the in-plane strain is shown in Fig. 8.

The number of layer-dependent magnetic coercive field and magnetization can be roughly explained by the domain wall rotation[30] and stress-induced magnetization[27] in epitaxial CFO layers of the composite film. If we carefully see the magnetic loops in PCP, PCPCP, and 11-layer films, hysteresis curves are shifted to left along the magnetic field axis in multilayer structures. This kind of shift in magnetic hysteresis loops can be understood based on the principle of magnetic exchange bias field. Magnetic exchange bias is the exchange interaction between the antiferromagnet (AFM) and ferromagnet (FM) at their interface. Since AFM have a small or no net magnetization, their spin orientation is only weakly influenced by a magnetic field. FM layer which is strongly exchange-coupled to the AFM will have its interfacial spins pinned. Reversal of the FM's moment will need more energy. The added energy implies a shift in the switching field and an increase in coercive field of the FM.[31] In highly strained epitaxial films, magnetic dead layer will be exist at the interface region because of the unrelaxed strain.[32] This magnetic dead layer with small net magnetization will act as the "AFM layer," which pin the spins of magnetic CFO at their interface. Therefore, this restricted rotation and movement of magnetic domain pinned by the dead layer in the interface give rise to the exchange bias and the increased coercive field. With the increase in the number of layer, the exchange bias will become strong because there are more interface exchange between the strained magnetic dead layer and the magnetic CFO. Besides, if we carefully measure the full width at half maximum (FWHM) of CFO peaks in 2θ-θ scan XRD patterns, the FWHM of CFO peaks increase from 0.34°, 0.39° to 0.41° for 3, 5, and 11-layer films. The increased FWHM may indicate the existence of short range strain in CFO phase. The short range strain can also act as the pin center in CFO layers, which will enhance the exchange bias and the coercive field. On the other hand, if we consider the energy contributions that control the easy axis of magnetization of the films. The energy can be written as[27]

$$E = K_1(\alpha_1^2\alpha_2^2 + \alpha_2^2\alpha_3^2 + \alpha_1^2\alpha_3^2) - \frac{3}{2}\lambda_{100}\sigma(\alpha_1^2\gamma_1^2 + \alpha_2^2\gamma_2^2 + \alpha_3^2\gamma_3^2) - 3\lambda_{111}\sigma(\alpha_1\alpha_2\gamma_1\gamma_2 + \alpha_2\alpha_3\gamma_2\gamma_3 + \alpha_1\alpha_3\gamma_1\gamma_3) + 2\pi M_S^2 v(f_z\alpha_3^2 + f_x\alpha_1^2 + f_y\alpha_2^2),$$

where the first term represents the cubic magnetocrystalline anisotropy, the second and third accounts for the magnetoelastic energy, and the last for the magetostatic energy of a thin film. We take the bulk values of CFO for the anisotropy constant ($K_1 = 3.9 \times 10^6$ erg/cm^3), saturated magnetization ($M_S = 0.534$ T), and magnetostriction coefficients ($\lambda_{100} = -590 \times 10^6$, $\lambda_{111} = 120 \times 10^6$). f_x, f_y, and f_z are the demagnetization coefficients, and v is the fraction of the film that is magnetic. α_1, α_2, and α_3 denote the direction cosines of M_S, and γ_1, γ_2, and γ_3 denote the direction cosines of stress axis with the three coordinate axes. The magnetostatic energy term is identical to $2\pi M_m^2$ with M_m being the measured moment. The magnetocrystalline energy term favors an easy axis along any of the ⟨100⟩ directions. Therefore, it does not favor an in-plane or out-of-plane magnetization and is neutral in this regard. Consequently, the easy axis will be tuned by the remaining magnetoelastic term, which will be positive or negative, depending on whether the in-plane strain is compressive or tensile. If the in-plane strain is compressive (tensile) this term is negative (positive), favoring an in-plane (out-of-plane) easy axis. Therefore, with an in-plane magnetic field, it is difficult to make the magnetization reach the saturated value in the CFO phase under an in-plane tensile strain. That is the reason that 11-layer film with largest in-plane compressive strain has large magnetization compare to 3-layer film. Furthermore, according to a general Le Chatelier's principle,[33] it is also well-known that the effect of stress on magnetization, coercive field, and permeability is mainly originated from the magnetostrictive nature of the materials. If a material has a positive magnetostrictive coefficient (λ), it will elongate when magnetized, reversely, its magnetization will increase under a tensile stress, and will decrease under a compressive stress. In the contrary, if a material has a negative magnetostrictive coefficient such as nickel[34] and cobalt ferrite,[28] its magnetization increases when a compressive stress is applied.

IV. CONCLUSION

Epitaxial PZT/CFO multilayer nanocomposite thin films have been successfully deposited on Nb:STO substrates, stress-induced ferroelectric polarizations, and dielectric behavior in the multiferroic films have been studied and the results are in line with our theoretical prediction. Our calculation and experimental data reveal that space charges exist in the films and influence the dielectric behavior and polarization but the amount of space charges in the films does not increase with the number of layers of PZT and CFO. The ferroelectric and ferromagnetic properties in the PZT/CFO

epitaxial films were also found to be modulated by the residual strain originated from coupling effect of the PZT/CFO interfaces. These results suggest that the magnetic, electric, and ME coupling effect may be tuned by the "strain engineering" in ferroelectric/ferromagnetic or other multiferroic superlattice.

ACKNOWLEDGMENTS

Financial support from the Hong Kong Polytechnic University Niche Area Funding 1-BB84 and the Hong Kong GRF grant (No. PolyU 5005/08P) are acknowledged. The author would like appreciate the fruitful discussion with Professor F.G. Shin and Dr. K.H. Chew.

[1]N. A. Spaldin and M. Fiebig, Science **309**, 391 (2005).
[2]J. F. Scott, Science **315**, 954 (2007).
[3]H. Zheng, J. Wang, S. E. Lofland, Z. Ma, L. Mohaddes-Ardabili, T. Zhao, L. Salamanca-Riba, S. R. Shinde, S. B. Ogale, F. Bai, D. Viehland, Y. Jia, D. G. Schlom, M. Wuttig, A. Roytburd, and R. Ramesh, Science **303**, 661 (2004).
[4]I. Levin, J. Li, J. Slutsker, and A. L. Royburd, Adv. Mater. **18**, 2044 (2006).
[5]Q. Zhan, R. Yu, S. P. Crane, H. Zheng, C. Kisielowski, and R. Ramesh, Appl. Phys. Lett. **89**, 172902 (2006); J. X. Zhang, J. Y. Dai, W. Lu, H. L. W. Chan, B. Wu, and D. X. Li, J. Phys. D **41**, 235405 (2008).
[6]C.-W. Nan, G. Liu, Y. Lin, and H. Chen, Phys. Rev. Lett. **94**, 197203 (2005).
[7]H. N. Lee, H. M. Christen, M. F. Chisholm, C. M. Rouleau, and D. H. Lowndes, Nature (London) **433**, 395 (2005).
[8]R. Ramesh and N. A. Spaldin, Nature Mater. **6**, 21 (2007).
[9]A. R. Chaudhuri, R. Ranjith, S. B. Krupanidhi, R. V. K. Mangalam, and A. Sundaresan, Appl. Phys. Lett. **90**, 122902 (2007).
[10]H. Zheng, J. Kreisel, Y.-H. Chu, R. Ramesh, and L. Salamanca-Riba, Appl. Phys. Lett. **90**, 113113 (2007).
[11]H.-C. He, J. Wang, J.-P. Zhou, and C.-W. Nan, Adv. Funct. Mater. **17**, 1333 (2007).
[12]J. X. Zhang, J. Y. Dai, W. Lu, and H. L. W. Chan, J. Mater. Sci. **44**, 5143 (2009).
[13]N. Ortega, A. Kumar, R. S. Katiyar, and J. F. Scott, Appl. Phys. Lett. **91**, 102902 (2007).
[14]N. Ortega, P. Bhattacharya, R. S. Katiyar, P. Dutta, A. Manivannan, M. S. Seehra, I. Takeuchi, and S. B. Majumder, J. Appl. Phys. **100**, 126105 (2006).
[15]T. Shimuta, O. Nakagawara, T. Makino, S. Arai, H. Tabata, and T. Kawai, J. Appl. Phys. **91**, 2290 (2002).
[16]N. A. Pertsev, A. G. Zembilgotov, and A. K. Tagantsev, Phys. Rev. Lett. **80**, 1988 (1998).
[17]P. Zubko, G. Catalan, A. Buckley, P. R. L. Welche, and J. F. Scott, Phys. Rev. Lett. **99**, 167601 (2007).
[18]P. Zubko, D. J. Jung, and J. F. Scott, J. Appl. Phys. **100**, 114113 (2006).
[19]I. Kanno, Y. Yokoyama, H. Kotera, and K. Wasa, Phys. Rev. B **69**, 064103 (2004).
[20]Y. H. Xu, *Ferroelectric Materials and Their Applications* (North-Holland, Amsterdam, 1991), p. 109.
[21]S. H. Oh and M. H. Jang, Appl. Phys. Lett. **72**, 1457 (1998).
[22]S. C.-K. Chow and V.-C. Lo, Theoretical Investigation of Electromechanical Responses in Ferroelectric Ceramics using Landau Khalatnikov Equation, J. Appl. Phys. (to be published).
[23]C. K. Wong and F. G. Shin, Am. J. Phys. **76**, 31 (2008).
[24]W. L. Zhong, Y. G. Wang, P. L. Zhang, and B. D. Qu, Phys. Rev. B **50**, 698 (1994).
[25]G. Liu, C.-W. Nan, Z. K. Xu, and H. Chen, J. Phys. D **38**, 2321 (2005).
[26]R. Kretschmer and K. Binder, Phys. Rev. B **20**, 1065 (1979).
[27]S. A. Chambers, R. F. C. Farrow, S. Maat, M. F. Toney, L. Folks, J. G. Catalano, T. P. Trainor, and G. E. Brown, Jr., J. Magn. Magn. Mater. **246**, 124 (2002).
[28]N. Wakiya, K. Shinozaki, and N. Mizutani, Appl. Phys. Lett. **85**, 1199 (2004).
[29]G. Hu, J. H. Choi, C. B. Eom, V. G. Harris, and Y. Suzuki, Phys. Rev. B **62**, R779 (2000).
[30]M. R. Fitzsimmons, P. Yashar, C. Leighton, K. I. Schuller, J. Nogués, C. F. Majkrzak, and J. A. Dura, Phys. Rev. Lett. **84**, 3986 (2000).
[31]J. Nogues and K. I. Schuller, J. Magn. Magn. Mater. **192**, 203 (1999).
[32]Y. Suzuki, Annu. Rev. Mater. Res. **31**, 265 (2001).
[33]B. D. Cullity, *Introduction to Magnetic Materials* (Addison-Wesley, Reading, MA, 1972), p. 266.
[34]B. Zhu, C. C. H. Lo, S. J. Lee, and D. C. Jiles, J. Appl. Phys. **89**, 7009 (2001).